Journal of Computer Assisted Tomography
11(1):2–6, January/February

Clinical Magnetic Susceptibility Mapping of the Brain

I. R. Young, S. Khenia, D. G. T. Thomas, C. H. Davis, D. G. Gadian, I. J. Cox, B. D. Ross, and G. M. Bydder

Abstract: A field mapping technique was used to detect changes in the local magnetic field in 14 tumors, five hematomas, one lacunar infarct, and two cases of multiple sclerosis. These changes were attributed to variations in the tissue susceptibility. A partial or complete rim of changed susceptibility was detected at the margin of five of the tumors and localized changes were seen within two of the tumors. All five hematomas displayed susceptibility effects. These were seen at the rim of the hematoma in all cases but central effects were also seen in four cases. One area of probable lacunar infarction also displayed susceptibility effects. The effects described may be due to the paramagnetic contribution of species such as deoxyhemoglobin, methemoglobin, free ferric iron, hemosiderin, and other breakdown products of blood. Local field inhomogeneities due to changes in tissue susceptibility have implications for magnetic resonance (MR) image interpretation and the performance of MR spectroscopy. **Index Terms:** Brain, infarction—Hematoma, cerebral—Magnetic resonance imaging.

Although techniques for mapping magnetic field variations are widely used to assess the homogeneity of magnets, their use in clinical practice has been limited and, to our knowledge, only one abstract describing the in vivo use of this technique has been published to date (1).

Apart from specific chemical shift effects, the local field experienced by any nucleus may vary as a result of (a) intrinsic inhomogeneities in the polarizing field and (b) the tissue magnetization that is induced by the polarizing field. The term magnetic susceptibility can be used to describe the latter effect. In general there are both diamagnetic and paramagnetic contributions to tissue susceptibility, the diamagnetic contribution tending to decrease the local field and the paramagnetic contribution tending to increase it. A fuller description of the various mechanisms involved is given by Abragam (2), together with its relevance to magnetic resonance (MR). In the studies described here we were particularly interested in the paramagnetic contribution that may be generated by various iron compounds.

A frequency (or phase) map that has been corrected for intrinsic inhomogeneities in the polarizing field (H_0) can be used to visualize the effects of variations in tissue susceptibility. In this article we describe the use of such a technique in 22 patients with disease of the brain. We observed effects that were attributed to field inhomogeneities generated by the accumulation of paramagnetic species within specific pathological regions.

MATERIALS AND METHODS

The (MR) system used in this study has been described previously (3). In this study two partial saturation sequences (4) were employed for the same slice in each patient. The first used a field echo to form an image and a phase map with an echo time (TE) of 33 ms. The second sequence used exactly the same gradients and data collection but was de-

From the GEC Hirst Research Laboratories, Wembley, Middlesex (I. R. Young and S. Khenia); the National Hospital for Nervous Diseases, London (D. G. T. Thomas and C. H. Davis); the Royal College of Surgeons, London (D. G. Gadian); and the NMR Unit, Hammersmith Hospital, London (I. J. Cox, B. D. Ross, and G. M. Bydder), England. Address correspondence and reprint requests to Dr. G. M. Bydder at NMR Unit, Hammersmith Hospital, Du Cane Road, London W12 OHS, England.

layed so that its TE was 113 ms. An image and a phase map were reconstructed from this image, and a third derived phase map displaying differences in phase between the first and second phase maps was also produced. The procedure was repeated using a large water phantom. The machine parameters were not changed between the patient's images and the phantom images. The patient's phase map could then be corrected for errors in B_0 by use of the reference map. The phase maps were displayed using a sawtooth gray scale (from black to white) corresponding to a phase difference of $\pm 180°$ with changes from black to white at the limits of this range.

The phase difference ϕD between signals from a voxel in the two phase images is given by

$$\phi D = \gamma \times \delta B \times t_d \quad (1)$$

where γ is the gyromagnetic ratio, δB is the difference in field between the voxel and a reference value, and t_d is the time between the two values of TE in the sequences used to compute the phase map. In this series t_d was 80 ms. This phase difference was displayed on the derived phase map. A 180° phase change on this image corresponded to a difference in field δB of 0.98 ppm. Phase differences can arise from chemical shift differences as well as field variations, but these are not a difficulty in the brain where there is no significant lipid signal and the concentrations of metabolites are too low to affect the images.

At least one spin echo (SE) 1,500/80, SE 1,500/120, or inversion recovery (IR) 1,500/500/44 image was also available in each case. These were obtained on the same system during the same examination. Computed tomography was also performed in each case using a Siemens Somatom II body scanner or a GE CT/T 8800 or 9800 scanner. The patients' final clinical diagnoses are summarized in Table 1. Histology was available in 11 of the 14 tumors but not in the cases of hematoma, lacunar infarction, or multiple sclerosis.

TABLE 1. *Clinical diagnoses*

Astrocytoma grade	I	1
	II	1
	III	2
	IV	1
	Low	2
Astrocytoma/oligodendroglioma		1
Oligodendroglioma		1
Metastasis		3
Probable craniopharyngioma		1
Meningioma		1
Hematoma		
Intracerebral hemisphere		3
pontine		1
cerebellar		1
Lacunar infarction		1
Multiple sclerosis		2

RESULTS

Normal Appearances

Images displayed low frequency changes attributable to inhomogeneity in B_0 (black and white bands) but little or no evidence of high frequency changes within the brain. The appearance of these bands was partially correctable by use of the phantom images.

Brain Tumors

In five of the 14 brain tumors local field variations were detected in all or part of the rim (Fig. 1). This corresponded in each case to an area of short T_1 (about that of white matter) on the IR 1,500/500/44 image and in two cases an area of relatively decreased signal intensity on the SE 1,500/80 images. Smaller areas displaying susceptibility effects were seen in two tumors (Fig. 2). These areas of changed susceptibility corresponded to regions of CT contrast enhancement in six of the seven cases.

Intracerebral Hematomas and Other Neurological Conditions

All five hematomas studied displayed susceptibility effects. These were ring shaped in all five and central in four. In one case an affected area was also seen in the intraventricular component of the hemorrhage (Fig. 3). Computed tomography displayed the hematoma in four cases. The susceptibility effects corresponded to the rim and central clot. In the fifth case CT showed only a low intensity region. The age of the hematoma in this case was estimated at 3 months.

In one case of probable bilateral lacunar infarction one lesion (Fig. 4) displayed susceptibility effects and two others did not.

In two cases of multiple sclerosis no change was observed within or at the margins of several plaques.

DISCUSSION

Phase maps were produced without difficulty in 22 patients and differences in lesion susceptibility were apparent in 11 cases. These were seen in all cases without correction for the polarizing magnetic field inhomogeneities although correction usually made them more obvious. The most obvious effects of susceptibility were seen in cases of intracerebral hematoma. We attribute these effects to the presence of paramagnetic breakdown products of blood. Similar but less obvious effects were seen at the margins of malignant tissues and within an infarct. These may also be due to hemoglobin degradation products.

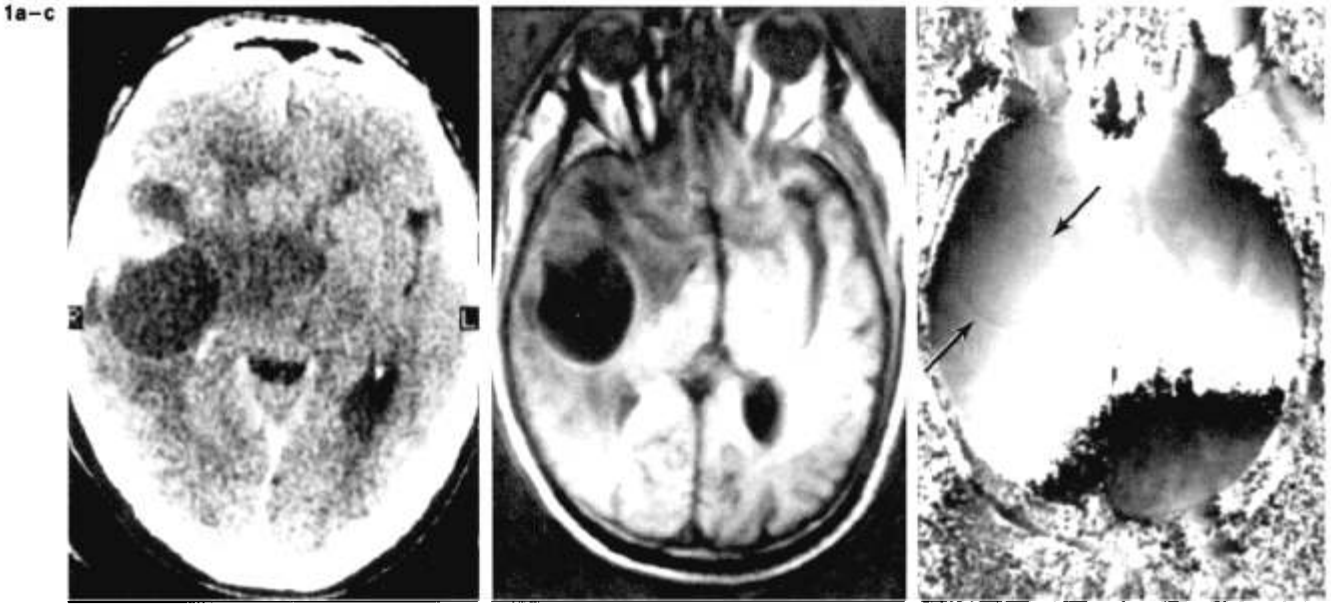

FIG. 1. Astrocytoma II: postcontrast CT scan **(a)**, IR 1,500/500/44 **(b)**, and phase map **(c)** images. A rim of changed susceptibility (arrows) is seen in **(c)** corresponding to the region of short T1 in **(b)** and slight rim enhancement in **(a)**. Low frequency changes **(c)**, black and white bands, are attributed to inhomogeneities in H_0.

Although most materials are diamagnetic, particular interest has surrounded the effects on MR signals of the paramagnetic contribution of species such as deoxyhemoglobin, methemoglobin, free Fe^{3+}, hemosiderin, and ferritin (5–8). These effects have generally been detected by virtue of the changes in relaxation times T1 and T2 (and indeed they form the basis of the use of contrast agents such as gadolinium–diethylenetriamine pentaacetic acid), but it is possible that paramagnetic species may produce susceptibility effects with relatively modest changes in T1 and T2 if sites for water binding are inaccessible.

The susceptibility contribution generated by paramagnetics (2) is given by

$$\chi_m = \frac{N m_0^2 \mu_o}{3kT} \qquad (2)$$

where χ_m is the molar susceptibility, m_0 is the magnetic moment, N is the number of molecules per unit volume, and μ_o is the magnetic permeability of free space.

Susceptibility differences between adjacent regions will generate field changes close to the boundary between the regions of the order of χ_m, which is of the order of 1 ppm for 10 mM of the

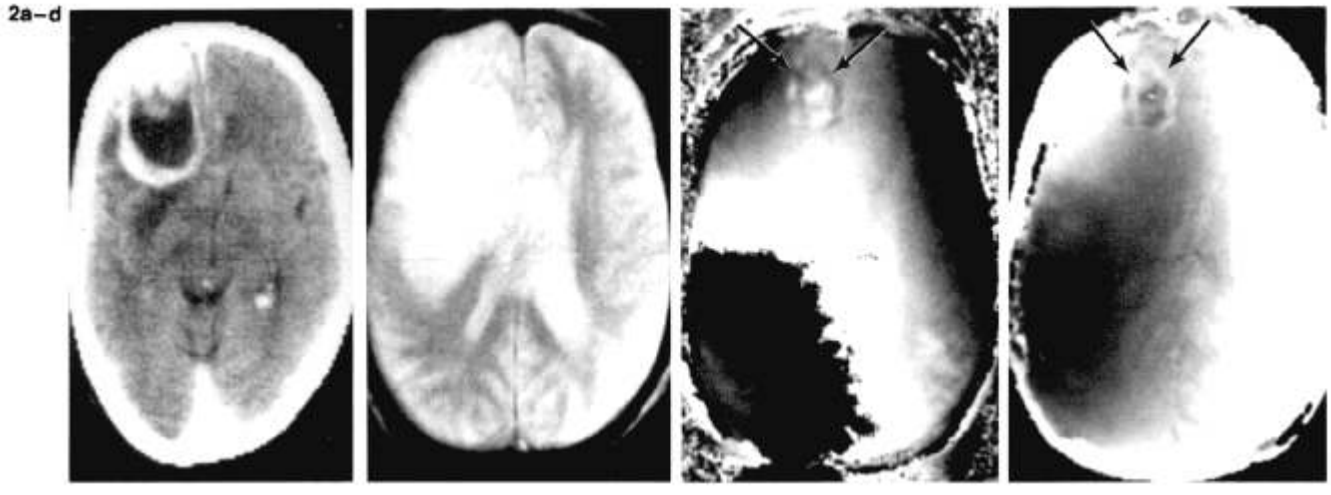

FIG. 2. Astrocytoma III: postcontrast CT scan **(a)**, PS 500/59:30° **(b)**, phase map **(c)**, and corrected map **(d)**. An area of changed susceptibility is seen in **(c)** and **(d)** (arrows) corresponding to the anterior region of CT enhancement **(a)**.

3a–d

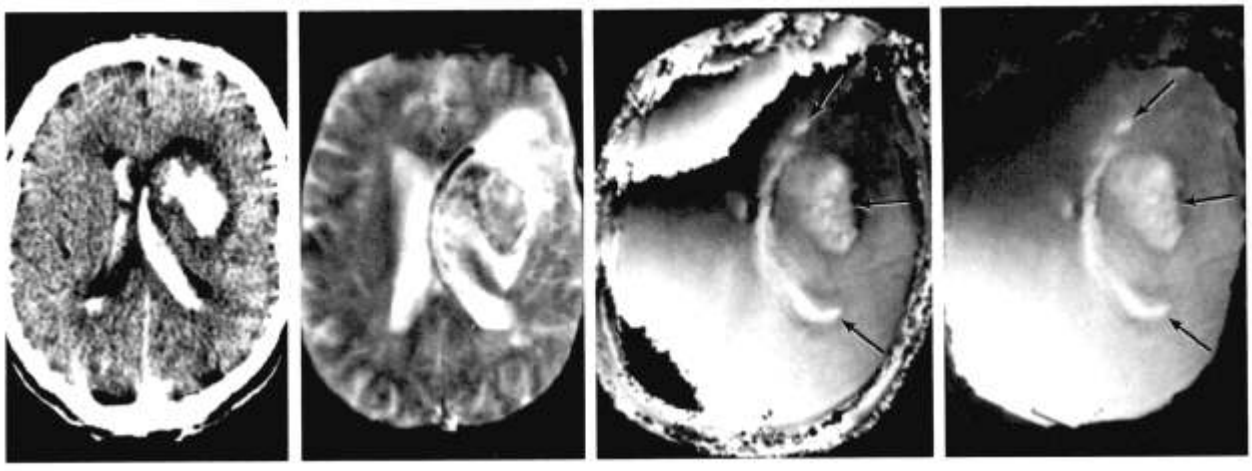

FIG. 3. Intracerebral and intraventricular hemorrhage: noncontrast CT scan **(a)**, PS 500/59:30° **(b)**, phase map **(c)**, and corrected phase map **(d)**. Changes in susceptibility are seen in the region of intracerebral and intraventricular hematoma (arrows, c and d).

paramagnetic species mentioned above. As the concentration of hemoglobin in normal blood is ~2.2 m*M* and there are four potential paramagnetic centers in each molecule, it is reasonable to expect field variations of the kind observed in the clinical results (up to 0.5 ppm). However, the precise nature of the field gradients will depend on several factors additional to the value of χ_m, such as the shape of the regions. A theoretical assessment of the susceptibility effects in vivo is therefore complicated by uncertainty about the spatial distribution of the paramagnetic species and by the fact that the paramagnetics may be intracellular, leading to the possibility of field gradients between individual cells in addition to the macroscopic gradients detected here.

It should be noted that, although the susceptibility maps use voxel phase differences as the contrast parameter, a different but related mechanism affects the signals in the normal field echo images. These are displayed after magnitude reconstruction (i.e., they show the intensity of the signal in each voxel and ignore the phase entirely). In these images susceptibility effects reduce T2*; T2* is given by the relationship (9)

$$\frac{1}{T2^*} = \frac{1}{T2} + \gamma \times \delta B \qquad (3)$$

where γ is the gyromagnetic ratio and δB is the field error across the volume of the voxel. The relationship was derived for, and generally applied to, populations of spins that have a Lorentzian distribution in the inhomogeneous field. Since the actual distribution is unknown and cannot practically be determined, it seems reasonable to use this well-established relationship.

Apart from any effects due to classic reduction of the time constant by dipole–dipole coupling with

4a,b

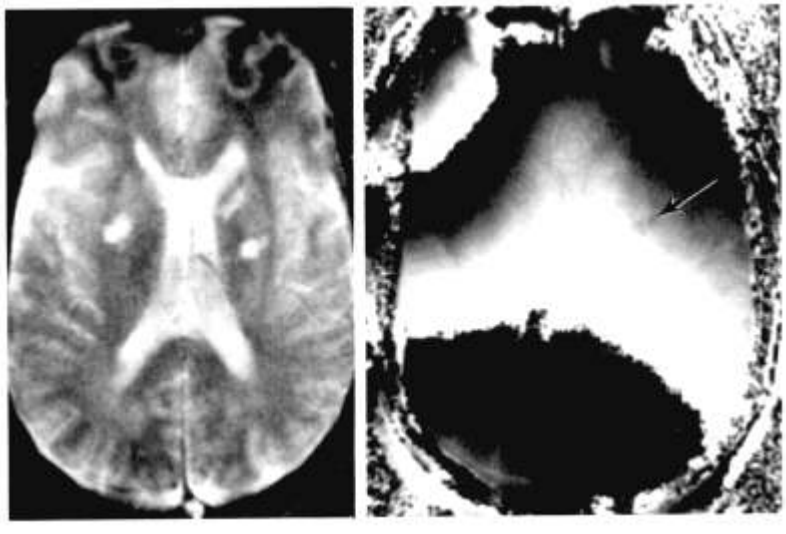

FIG. 4. Lacunar infarctions: PS 500/120:30° **(a)** and phase map **(b)**. Area of changed susceptibility is seen in **(b)** (arrow).

the paramagnetic nuclei, the signals observed in the field echo images also reflect the dephasing of the voxels due to field inhomogeneities inside them, whereas the differences in the phase maps reflect the net phase of the whole voxels. Apart from magnetic field effects, coherent flow phenomena can also cause voxel phase shifts. Random flow patterns (such as diffusion on the microscopic scale) on the other hand only result in reduction of the signal amplitude. In the magnitude images, changes with high spatial frequencies (such as some of those shown in the phase maps) have a particularly significant effect, because they occur inside the volume of a voxel. The net result of significant fluctuations in field echo images is thus a drop in T2*. Note also that this effect differs from the mechanism involving diffusion through gradients at cellular dimensions, where the T2 contribution is dependent on B_0^2. If it is intended to emphasize these changes, it may be better to increase the slice width (because it is generally the biggest single voxel dimension) rather than reduce it.

Chemical shift effects (as observed in spectroscopy) are also due to local field perturbations, and so the presence of materials such as fat results in substantial sharp shifts in the field maps. In the brain, however, lipid signals are insignificant so that this potential source of confusion with susceptibility changes is not present. Susceptibility, as described here, is a bulk effect, however, and, if changes in it are present, they will shift all the lines.

Mapping of susceptibility effects provides another image parameter that is of value in the understanding of MR images. It is also of importance in relation to MR spectroscopy, because significant local field variations may make it difficult to optimize the field homogeneity that is so important for high resolution spectra. For example, the region of a tumor of metabolic interest may be the outer ring, which displays contrast enhancement on CT, yet this was the site displaying local field gradients in approximately one-third of the cases studied in this series.

Acknowledgment: We thank the Rank Foundation, the Medical Research Council, and the Department of Health and Social Security for their support.

REFERENCES

1. Faul D, Arbart J, Margosian P. Quick measurement of magnetic field variations within the body. *Radiology* 1984; 153:303–4.
2. Abragam A. *The principles of nuclear magnetism*. Oxford: Clarendon Press, 1961:1–4.
3. Young IR, Bailes DR, Burl M, et al. Initial clinical evaluation of a whole body nuclear magnetic resonance (NMR) tomograph. *J Comput Assist Tomogr* 1982;6:1–18.
4. Bydder GM, Young IR. Clinical use of the partial saturation and saturation recovery sequences in MR imaging. *J Comput Assist Tomogr* 1985;9:1020–32.
5. Dodd NJF, Silcock JM. Electron spin resonance study of changes during development of solid Yoshida tumour. II. Paramagnetic metal ions. *Br J Cancer* 1976;34:556–65.
6. Gadian DG, Proctor E, Williams SR, Cox IJ, Young IR. Spectral resolution in metabolic studies of the brain [Abstract]. In: *Fourth annual meeting of the Society of Magnetic Resonance in Medicine. August 19–23, 1985, London, England.* Berkeley: Society of Magnetic Resonance in Medicine, 1985:273–4.
7. Gomori JM, Grossman RI, Goldberg HI, Zimmerman RA, Bilaniuk LT. Intracranial hematomas: imaging by high-field MR. *Radiology* 1985;157:87–93.
8. Bradley WG Jr, Schmidt PG. Effect of methemoglobin formation on the MR appearance of subarachnoid hemorrhage. *Radiology* 1986;156:99–103.
9. Abragam A. *The principles of nuclear magnetism*. Oxford: Clarendon Press, 1961:49–51.